

NJC

Accepted Manuscript



This is an *Accepted Manuscript*, which has been through the Royal Society of Chemistry peer review process and has been accepted for publication.

Accepted Manuscripts are published online shortly after acceptance, before technical editing, formatting and proof reading. Using this free service, authors can make their results available to the community, in citable form, before we publish the edited article. We will replace this *Accepted Manuscript* with the edited and formatted *Advance Article* as soon as it is available.

You can find more information about *Accepted Manuscripts* in the [Information for Authors](#).

Please note that technical editing may introduce minor changes to the text and/or graphics, which may alter content. The journal's standard [Terms & Conditions](#) and the [Ethical guidelines](#) still apply. In no event shall the Royal Society of Chemistry be held responsible for any errors or omissions in this *Accepted Manuscript* or any consequences arising from the use of any information it contains.



www.rsc.org/njc

ARTICLE

An electrochemical immunoassay based on trepang-like gold electrode and nanogold functionalized flower-like hierarchical carbon materials with improved sensitivity

Cite this: DOI: 10.1039/x0xx00000x

Received 00th January 2012,
Accepted 00th January 2012

DOI: 10.1039/x0xx00000x

www.rsc.org/

Kaiqing Wu^a, Yan Zhang^a, Mei Yan^a, Shenguang Ge^b, Jinghua Yu^{a,*}, Xianrang Song^c

A novel electrochemical immunosensor for detection of carcinoembryonic antigen (CEA) was developed by using nanogold functionalized flower-like hierarchical carbon material (AuNPs/FCM) labeled with horseradish peroxidase-secondary antibodies as signal amplification label. The amplified detection was achieved by the increased HRP-electrocatalyzed reduction of hydrogen peroxide. In order to construct the base of the immunosensor, a hybrid platform was generated by the electrostatic attraction between poly (diallyldimethylammonium chloride) functionalized graphene (G-PDDA) and three-dimensional trepang-like gold (3D-TG). The platform with excellent electronic properties, stability, bioactivity and large surface area, was served as an effective matrix for CEA-primary monoclonal antibodies. Subsequently, a sandwich-type immunocomplex of 3D-TG/G-PDDA and AuNPs/FCM was formed based on the immunoreaction of antibody-antigen in the presence of CEA. Enhanced sensitivity was obtained by combining the advantages of excellent electrical conductivity and bioactivity of the hybrid sensor platform with the multilabel signal amplification. Under optimal conditions, our strategy displayed excellent analytical performance for the detection of CEA ranging from 0.0001 to 50 ng·mL⁻¹ with a detection limit of 0.026 pg·mL⁻¹. The new proposed method provides a new promising platform for the design of the highly sensitive detection method, showing great promise for clinical immunoassays.

Introduction

Sensitive detection of disease-related proteins is essential for many areas of modern biochemical and biomedical research. In particular, the sensitive detection of cancer biomarkers shows great importance for the clinical cancer screening, disease diagnosis, and monitoring.¹⁻³ Immunoassay based on the highly specific interaction between antigen and antibody is one of the most important methods for the specific analysis of those cancer biomarkers. To date, several conventional immunoassay procedures including radio-immunoassays,⁴ enzyme-linked immunosorbent assay (ELISA),^{5,6} fluorescence immunoassay,⁷ surface-enhanced Raman scattering,⁸ and piezoelectric immunosensors,⁹ have been already reported for cancer biomarkers detections, but some of them suffer from

drawbacks, such as radiation hazards, long analysis times, or the need for sophisticated instrumentations.¹⁰ Therefore, electrochemical immunosensors^{11,12} as an alternative to the conventional immunoassay procedures, have shown great promise because of simple instrumentation, good portability, high sensitivity, low cost and fast response time.

In order to develop a sensitive and high-performance immunosensor, signal amplification and noise reduction are required. To fulfill the goal, various labels such as nanomaterials,^{13,14} fluorescent particles or compounds^{15,16} and enzymes^{17,18} have been developed to monitor antibody-antigen interaction. Enzymes, such as esterase, alkaline phosphatase, and horseradish peroxidase (HRP), are the most common labels employed for signal amplification. In addition, HRP-labeled antibody (HRP-McAb₂) is popular used in

immunosensor due to its small size and high stability to the chemical modifications.¹⁹ As far as we know, the sensitivity of the immunosensor was related to the amounts of enzyme loading. Therefore, it is significant to increase the enzyme loading in an immunosensor. To date, various nanomaterials have been used as carriers to load enzymes and antibodies, including nanogold (AuNPs), silica nanoparticles, carboxylated magnetic beads and carbon nanomaterials.^{20,21} The excellent properties of nanomaterials, such as good biocompatibility, high surface-to-volume ratio, offer outstanding prospects for interfacing biological recognition events with electronic signal transduction. Due to the good biocompatibility and easy functionalization with biomolecules, AuNPs have been extensively applied as a favorable nanocarrier of signal molecules in immunoassays.²² For example, AuNPs can be modified with enzymes or enzyme labeled antibodies to prepare multi-enzyme nanoprobe and so as to construct sensitivity enhanced electrochemical immunoassays for low-level proteins. However, due to the big size of protein, these probes can only load around 10 enzymes which greatly limit their amplification performance.²³ Hence, flower-like hierarchical carbon material (FCM), as a novel carbon nanomaterial with large surface area and excellent catalytic properties, may have advantages to conjugate more biomolecules. Thus the AuNPs/FCM nanocomposites could be beneficial to develop highly sensitive immunosensor. As far as we know, this is the first report that applied hierarchical carbon material as nanocarrier to load HRP-McAb₂ to establish electrochemical immunosensor for CEA detection.

To perform as an excellent sandwich-type immunosensor, stability and activity of the immobilized antibodies on platform have been a longstanding goal. Various nano-materials have been employed to modify the biosensing platform, aimed at improving the sensing performance.^{24,25} Recently, much attention has been centered on graphene due to its fascinating two-dimensional structure, unusual electrochemical properties, large accessible surface area, as well as good biocompatibility. The unique properties of graphene, especially good electronic conductivity and high surface area, make it a promising interface material for sensor applications,^{26,27} especially for electrochemical biosensors. For example, Qi et al²⁸ have reported a sensitive label-free electrochemical immunosensor based on palladium/graphene, and it has exhibited good selectivity and long-term stability and high sensitivity for the detection of alpha fetoprotein. Furthermore, metal hybrid graphene exhibited much more excellent properties than the graphene alone. Three-

dimensional trepan-like gold (3D-TG), hierarchical architectures with porous structures, has attracted considerable attention due to its high surface-to-volume reaction, high conductivity and biocompatible in recent years. These amazing properties make 3D-TG become an attractive material for the immobilization of enzymes and biomolecule, and the construction of biosensors.²⁹ Therefore, the 3D-TG hybrid graphene may exhibit good electrochemical performance once be employed as an electrode support.

With the development of the living standard, human tend to pay more and more attention to the diseases, especially the cancer, which affect their health. Carcinoembryonic antigen (CEA), a polysaccharide-protein complex, is one of the most studied tumor markers associated with liver cancer, colon cancer, colorectal cancer, breast cancer, exists in endoblast origin digestive system cancer. Its levels may reflect the disease progression or regression status. So that accurate and fast detection of the CEA is of significance for monitoring and screening disease recurrence, and can improve the long term survival of cancer patients. In this paper, a novel electrochemical immunosensor for the detection of CEA was constructed. To combine the negative charged 3D-TG, the functionized graphene by PDDA (3D-TG/G-PDDA) with positive charge was first synthesised. Then the CEA-primary monoclonal antibodies (CEA-McAb₁) were dropped onto 3D-TG/G-PDDA nanocomposites modified electrode for subsequent immune-recognition between CEA-McAb₁ and CEA. Subsequently, AuNPs/FCM were mixed with HRP-McAb₂ to generate bioconjugates. The reaction is based on the interaction between NH₂ or SH groups on the HRP-McAb₂ biomolecules and AuNPs. In addition, the amplified sensitivity was enhanced by using the novel carbon material labeled with HRP-McAb₂. The limit of detection, detection sensitivity and linear range were all improved with the newly established system. Therefore, this novel immunosensor may be used to develop sensitive and specific cancer diagnostic tools.

Experimental section

Materials and methods

CEA-McAb₁, HRP-McAb₂, and CEA standards solutions were purchased from Shanghai Linc-Bio Science Co. Ltd. (Shanghai, China). 1-ethyl-3-(3-(dimethylamino) propyl) carbodiimide hydrochloride (EDC), N-hydroxysuccinimide (NHS), PDDA, bovine serum albumin (BSA, 96–99%), gold chloride (HAuCl₄·4H₂O), thionine (TH), trisodium citrate dehydrate, zinc nitrate, methylbenzene (MB), 2,2'-azino-bis-(3-ethylbenz-thiazoline-6-

sulfonic acid) (ABTS) were obtained from Sigma-Aldrich Chemical Co. (St. Louis, MO, USA). 100 nm-thick white gold foils (Au/Ag alloy, 50:50 wt%) were obtained from Monarch. Hydrogen peroxide (H_2O_2 , 30%, w/v) was obtained from Chemical Reagent Co. (Tianjin, China). Phosphate buffer saline (PBS, $10 \text{ mmol}\cdot\text{L}^{-1}$), made from Na_2HPO_4 , KH_2PO_4 , and H_3PO_4 , was employed as supporting electrolyte. The aqueous solutions unless indicated were prepared with ultra-pure water which was obtained from a Lichun water purification system ($\geq 18 \text{ M}\Omega\cdot\text{cm}$).

Scanning electron microscope (SEM) images were obtained using a QUANTA FEG 250 thermal field emission scanning electron microscopy (FEI Co., USA). Transmission electron microscope (TEM) images were obtained from a JEOL JEM-1400 microscope (Japan). Electrochemical experiments, including cyclic voltammetry (CV) and differential pulse voltammetry (DPV), were performed on a CHI 660D electrochemistry workstation (Shanghai CH Instruments Co., China). Electrochemical impedance spectroscopy (EIS) was performed on an IM6x electrochemical station (Zahner, Germany). Infrared (IR) spectra were recorded using a Nicolet 400 Fourier transform infrared spectrometer (Madison, WI). The phase characterization was performed by X-ray diffraction (XRD) using a D8 advance diffractometer system equipped with $\text{Cu K}\alpha$ radiation (Bruker Co., Germany).

Synthesis of G-PDDA and 3D-TG

The G-PDDA nanocomposite was prepared by the chemical reduction of graphite oxide (GO, the detail information on the synthesis of GO can be found in the Electronic Supplementary Information) with hydrazine under the protection of PDDA according to the work of Liu et al.³⁰ Briefly, 2 mL GO ($2 \text{ mg}\cdot\text{mL}^{-1}$) was mixed with 10 mL PDDA aqueous solution (1.0%) and sonicated for 30 min to give a homogeneous suspension. Subsequently, the resulting mixture was further treated with 0.5 mL hydrazine hydrate and allowed to react for 24 h at 90°C . Finally, the black PDDA-functionalized graphene (G-PDDA) was collected by filtration and further washed with water for five times and redispersed in 4 mL ultra-pure water with mild sonication.

Seed-mediated growth of gold nanostructure of various morphologies is often carried out in aqueous solution by using HAuCl_4 gold precursor and hydroxylamine/ascorbic acid as the reductant.³¹ Therefore, AuNPs seeds was first prepared by using NaBH_4 as the reductant and stabilized with sodium citrate according to the previous reported literature.³² Then 5 mL of AuNPs seeds solution was added into 10 mL of 1% $\text{HAuCl}_4\cdot 4\text{H}_2\text{O}$ with vigorous

stirring. After stirring for 1 min, 60 mg of AA powder was added and kept stirring for 1 h. The final as-prepared products were centrifuged and washed using water and ethanol, respectively.

Synthesis of FCM

The FCM was synthesized according to the previous report with slight modified.³³ To obtain the FCM, the ZnO template with flower-like structure was synthesized firstly. Briefly, 1.5 g of zinc nitrate hexahydrate and 3.5 g of trisodium citrate dehydrate were firstly dissolved in 100 mL of ultra-pure water under stirring. Then 20 mL of NaOH solution ($1.25 \text{ mol}\cdot\text{mL}^{-1}$) was added into the mixed solution and keep stirring for 3 h at room temperature. Subsequently, the flower-like ZnO (F-ZnO) were centrifuged for 5 min at the rate of 10000 rpm and repeated for five times. In the end, the product can be obtained with the procedure of drying at 100°C for one night.

The FCM was prepared as follows: 0.10 g of pitch was dissolved in 20 mL of MB by sonication for 1 h to get the clarifying solution. Then 0.40 g of prepared F-ZnO was dispersed in 50 mL of MB under violently stirring. Afterwards, the pitch solution was pulled into the F-ZnO solution slowly under stirring. After stirred for 5 h, a rotary evaporator was employed to get rid of the solvent MB of the mixture solution. Then the brown solid followed by heating at 500°C for 2 h in a N_2 atmosphere. Finally, the FCM was obtained after the removal of F-ZnO template by hydrochloric acid treatment.

Bioconjugation of AuNPs/FCM with HRP-Ab₂

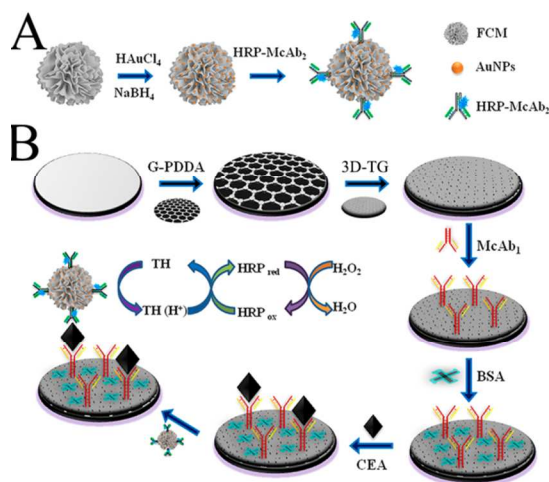
As shown in Scheme 1A, 2 mg FCM was first carboxyl functionalized and shortened by sonicating in a mixture of concentrated HNO_3 and H_2SO_4 (v/v, 1:3) for 4 h followed by extensive washing in deionized water until the filtrate was at neutral pH. Then, 600 μL of HAuCl_4 aqueous solution (w/w, 1%) was added into the purified FCM mentioned above, and incubated for 2 h with slightly stirring at room temperature. Then the AuCl_4^- ions adsorbed on the surface was reduced to AuNPs with the help of $0.01 \text{ mol}\cdot\text{L}^{-1}$ NaBH_4 solution. After centrifugation and washing by ultra-pure water, the obtained AuNPs/FCM nanocomposites were stored at 4°C before use.

500 μL of HRP-McAb₂ ($50 \mu\text{g}\cdot\text{mL}^{-1}$) was added into 1 mL AuNPs/FCM ($1 \text{ mg}\cdot\text{mL}^{-1}$) nanocomposite suspension, and the mixture was continuously stirred at 4°C . After being incubated for 10 h, the mixture was washed with PBS buffer, then centrifuged at 10000 rpm for 3 min, repeatedly washed and centrifuged three times. Following that, 1% BSA solutions was added into the precipitation for 40 min at room temperature to eliminate non-specific binding

effects and block the remaining active sites. The obtained HRP-McAb₂/AuNPs/FCM was stored at 4 °C until use.

Fabrication of the immunosensor

For electrochemical catalytic measurements, a glassy carbon electrode (GCE) was employed as working electrode. A platinum wire and KCl saturated Ag/AgCl electrode was used as the counter electrode and reference electrode, respectively. Prior to the preparation procedure, the GCE (Φ¼ 4 mm) was firstly polished with 0.3 and 0.05 μm alumina slurry to obtain a mirror-like surface, followed by successive sonication with ultra-pure water and ethanol, and then dried at room temperature. The pretreated GCE was firstly coated with 5 μL G-PDDA homogeneous suspensions and allowed to dry at room temperature. The modified GCE was then immersed in 3D-TG solution for 2 h to capture 3D-TG. Next, the modified working electrode was incubated with CEA (5 μL, 25 μg·mL⁻¹) for 1 h, followed by washing with PBS buffer to remove unspecific physically adsorption. Subsequently, 1% BSA solution was placed onto the electrode for 1 h at room temperature to block the remaining active sites against nonspecific adsorption. After another washing with PBS, the resulting immunosensor was obtained and stored at 4 °C prior to use. Part of this fabrication process of the electrochemical immunosensor is illustrated in Scheme 1B.



Scheme 1 Fabrication process of (A) HRP-McAb₂/AuNPs/FCM and (B) measurement protocol of the electrochemical immunosensor.

Measurement procedure

Electrochemical measurements of this immunosensor toward CEA samples or standards solutions were carried out through a sandwich-type immunoassay mode using HRP-McAb₂/AuNPs/FCM as tracers

and H₂O₂ as enzyme substrates. The immunosensor was firstly incubated with the mixture of CEA standard solutions (10 μL) with various concentrations for 40 min at room temperature. After being formed with the antigen–antibody immunocomplex, the electrodes were washed with 0.1 M PBS (pH 7.4) to remove unbounded CEA molecules. Then HRP-McAb₂/AuNPs/FCM (5 μL) was dropped onto the modified electrode for another 40 min at room temperature to form the sandwiched immunocomplex. Ultimately, the electrochemical detection was performed in a pH 7.4 PBS buffer solution containing 50 μmol·L⁻¹ TH and 3 mmol·L⁻¹ H₂O₂. Ultimately, differential pulse voltammetry (DPV) from -0.65 to 0.05 V with a pulse amplitude of 50 mV and a pulse width of 50 ms was performed to record the electrochemical responses for simultaneous measurement of CEA in PBS (pH 7.4).

Results and discussion

Characterization of F-ZnO and AuNPs/FCM

In this work, the synthesis of FCM was based on the template of F-ZnO. To verify the morphology and the size of the as-prepared F-ZnO, SEM characterization was in use. As shown in Fig. S1A, the F-ZnO owns a flower-like structure with an average diameter of ~1.5 μm. The powder XRD pattern of F-ZnO was shown in Fig. S1B. It confirmed a well crystallized structure, and all the diffraction peaks can be readily indexed to hexagonal P63mc F-ZnO phase (JCPDS 36-1451). As shown in Fig. S1C, the carbon material was covered on the F-ZnO. After being treated by hydrochloric acid, ZnO was removed and FCM was appealed as a result. Fig. 1A shows the corresponding SEM images of as-prepared FCM. It is clearly seen that the FCM exhibits a uniform flower-like structure like ZnO template. After the in situ growth of nanogold, numbers of homogeneous and dense coverage of AuNPs can be seen on the FCM surface (Fig. 1B). The crystallographic structure of the FCM and AuNPs/FCM were investigated by XRD. As shown in Fig. 1C, XRD patterns of FCM (curve a) exhibits broad diffraction peaks centered at around 25°, ascribing to the (002) crystal planes of graphitic carbon; The prominent peaks in the XRD pattern of AuNPs/FCM (curve b) at 2θ values of about 38.2°, 44.57° and 64.69° were assigned to the (111), (200) and (220) crystallographic planes of AuNPs, respectively (JCPDS card No 004-0784), suggesting that AuNPs had been successfully deposited on the surface of FCM.

Characterization of G-PDDA and 3D-TG

Given that the 3D-TG was negatively charged, the PDDA-functionalized graphene was in use for the formation of 3D-TG/G-PDDA hybrid architecture. Fig. 2A shows the TEM image of graphene nanosheets, clearly illustrating typical flake-like wrinkled shapes of graphene with irregular size. FT-IR spectroscopy was employed to investigate the reduction and the functionalization process. Compared with GO, as shown in Fig. 2B curve a, the absence of oxo-groups (C=O, C-O) in pure G indicated complete reduction of GO. The absorption bands at 2918 cm^{-1} (CH_n), 1633 cm^{-1} (C=C) and 1442 cm^{-1} (C=C) corresponded to the characteristic bands of PDDA, indicating the functionalization of graphene with PDDA.³⁴

Typical SEM image of 3D-TG was shown in Fig. 2C. As shown, 3D-TG displays a type of flower-like morphology after the addition of AA solution, with a $250 \pm 30\text{ nm}$ sized structure. Such metallic structures with hierarchical morphology were of great interest for a number of technological applications. Furthermore, it demonstrated that the structures were beneficial for the adsorption of biomolecules.

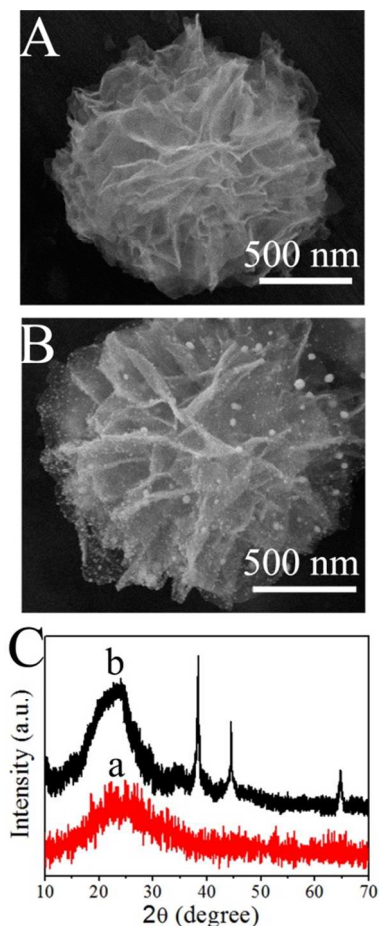


Fig. 1 (A) SEM image and FCM; (B) SEM image of AuNPs/FCM; (C) XRD of the (a) FCM and (b) AuNPs/FCM.

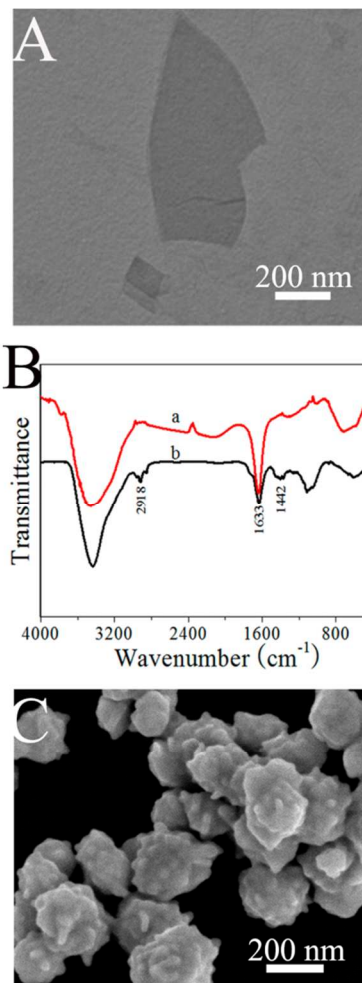


Fig. 2 (A) TEM image of graphene; (B) FT-IR of (a) graphene and (b) G-PDDA; (C) SEM image of 3D-TG.

EIS characterization

According to our understanding, EIS is a sensitive and reliable method to study the interface properties of chemically modified electrode surface. The respective semicircle diameter corresponds to the electron transfer resistance at the electrode surface. In this work, EIS was used to characterize the assembly of the immunosensor. Fig. 3A exhibited the Nyquist plots of the different modified electrodes in a background solution of $5.0\text{ mmol}\cdot\text{L}^{-1}$ $[\text{Fe}(\text{CN})_6]^{3-/4-}$ containing $0.1\text{ mol}\cdot\text{L}^{-1}$ KCl, and the frequency range is at 100 mHz to 10 kHz at 220 mV . As shown in Fig. 3 A, the Nyquist plot (curve a) of bare electrode exhibited a small semicircle domain. After dropping $5\ \mu\text{L}$ G-PDDA on the GCE, the corresponding Nyquist plot (curve b) showed a semicircle with a slightly smaller diameter. It revealed that the G-PDDA was an excellent electric conducting material to accelerate the electron transfer. Furthermore, when the 3D-TG was introduced, a much lower resistance than the former was shown as

curve c, indicating that the introduction of the 3D-TG was highly beneficial to the electron transfer. Subsequently, when the electrode was conjugated with McAb₁, the R_{ct} increased (curve d), which suggested that the McAb₁ was successfully immobilized on the surface and formed an additional barrier and blocked the electron exchange between the redox probe and the electrode. Similarly, BSA and CEA could all resist the electron transfer kinetics of the redox probe at the electrode surface, resulting in the increasing impedance of the electrode as well (curves e and f), which were caused by the nonconductive properties of biomacromolecule. At last, after the HRP-McAb₂/AuNPs/FCM interacted with CEA, the resistance sequentially increased (curve g). The results showed that the multienzyme-antibody functionalized FCM was successfully immobilized on the surface.

Electrochemical behaviors of the immunosensors

A biocomposite is formed by combination of two or more phases of different natures. It acts not only as a support for the immunologic material but also as a transducer. For the immunosensor fabrication, McAb₁ was firstly attached onto 3D-TG/G-PDDA modified GCE. As shown in Fig. 3B, the cyclic voltammograms (CV) at 3D-TG/G-PDDA/GCE (curve a) and McAb₁/3D-TG/G-PDDA/GCE (curve b) did not show any detectable signal in pH 7.4 PBS buffer. Upon adding 50 $\mu\text{mol}\cdot\text{L}^{-1}$ TH and 3 $\text{mmol}\cdot\text{L}^{-1}$ H₂O₂ to the PBS buffer, a pair of stable and well defined redox peaks was appeared (curve c), which corresponded to the CV of McAb₁/3D-TG/G-PDDA/GCE. The redox peak was attributed to the electrochemical oxidation and reduction of TH, a good electron mediator with good electroactivity. When the immunosensor was incubated with CEA, the change in response (data not shown) removed slightly compared to curve c. After the HRP-Ab₂ was reacted with the immunosensors, the resulting HRP-McAb₂/CEA/McAb₁/3D-TG/G-PDDA/GCE displayed an obvious increase in electro-catalytic reduction current (curve d) because of the introduction of HRP onto the electrode surface. The HRP could retain high enzymatic catalytic activity and effectively shuttle electrons from the base electrode surface to the redox center of HRP. However, a more significant increased reduction current at the immunosensor was observed once the HRP-Ab₂ was replaced by HRP-McAb₂/AuNPs/FCM (curve e) during the sandwich immunoreactions, respectively. It can be seen that the immunosensor exhibited higher sensitivity using HRP-McAb₂/AuNPs/FCM as probes. The achieved amplification of signal may be ascribed to a large amount of enzymes loaded on the FCM, which displayed a high surface-to-volume ratio (the detail

information on the determination of the amount of active HRP can be found in the Electronic Supplementary Information). In addition, AuNPs with higher capability of electron transfer could effectively transfer electrons from the base electrode surface to the redox center of HRP. Meanwhile the nanoparticles can further amplify the specific surface area and enhance the sensitivity of the immunoassay.

The signal amplification was also confirmed by DPV measurement. As shown in Fig. S2A, a higher catalytic current was observed at HRP-McAb₂/AuNPs/FCM/CEA/McAb₁/3D-TG/G-PDDA/GCE (curve a) compared with HRP-McAb₂/CEA/McAb₁/3D-TG/G-PDDA/GCE (curve b) since HRP-McAb₂/AuNPs/FCM as a detection antibody could introduce more HRP on the electrode surface. This phenomenon could also be seen even with G-PDDA/GCE without 3D-TG modification. The catalytic current obtained from HRP-McAb₂/AuNPs/FCM (curve c) at CEA/McAb₁/G-PDDA/GCE was 2.5-fold higher than that from HRP-McAb₂ (curve d). The achieved amplification was mainly ascribed to the excessive enzyme present in the AuNPs/FCM label when HRP-McAb₂/AuNPs/FCM was used as a detection antibody. Furthermore, we explored the role of 3D-TG/G-PDDA as a sensor platform. Compared to CEA/McAb₁/G-PDDA/GCE and CEA/McAb₁/3D-TG/G-PDDA/GCE, the catalytic current increased from 5.79 μA (curve c) to 15.88 μA (curve a) when HRP-McAb₂/AuNPs/FCM was used as a detection antibody. Also, the responses increased from 2.54 μA at CEA/McAb₁/G-PDDA/GCE (curve d) to 4.57 μA at CEA/McAb₁/3D-TG/G-PDDA/GCE (curve b) when traditionally labeled HRP-McAb₂ was used. These data illustrated that although G-PDDA/GCE could also specifically capture Ab₁, much lower peak currents and slight positively shifted potentials were observed compared to those at 3D-TG/G-PDDA/GCE. The presence of 3D-TG not only obviously increased the surface area to capture more antibodies on the electrode surface but also accelerated electron transfer. On the basis of the dual amplification of 3D-TG and HRP-McAb₂/AuNPs/FCM, the catalytic current at HRP-McAb₂/AuNPs/FCM/CEA/McAb₁/3D-TG/G-PDDA/GCE enhanced about 6-fold in comparison with that at HRP-McAb₂/CEA/McAb₁/G-PDDA/GCE without 3D-TG modification and AuNPs/FCM labelling.

A series of control experiments were conducted in PBS containing TH and H₂O₂ by DPV measurements. As shown in Fig. S2B, both the McAb₁/G-PDDA/GCE (a) and McAb₁/3D-TG/G-PDDA/GCE (b) presented small signals. A slight increase of catalytic currents was obtained when the McAb₁/3D-TG/G-PDDA/GCE was directly exposed to HRP-McAb₂ (c) or HRP-McAb₂/

AuNPs/FCM (e) without preincubation in a CEA solution. These responses might result from nonspecific adsorption on the electrode. However, after incubating with 5 ng mL^{-1} CEA, the responses of both obtained HRP-McAb₂/CEA/McAb₁/3D-TG/G-PDDA/GCE (d) and HRP-McAb₂/AuNPs/FCM/CEA/McAb₁/3D-TG/G-PDDA/GCE (f) increased greatly. Although the incubation of HRP-McAb₂/AuNPs/FCM (e) showed a much higher background signal than that of HRP-McAb₂ (c), the signal-to-noise ratio (S/N) before and after incubating with CEA from HRP-McAb₂/AuNPs/FCM (f/e) was much larger than that from HRP-McAb₂ (d/c), thus amplifying the detection signal.

Condition optimization

The incubation time was an important parameter affecting the analytical performance of immunoassay. Before the exploration, considering the practical feasibility in real life, all the experiments in this study were carried out at room temperature. Thus the DPV response of the immunosensor toward 5 ng mL^{-1} CEA increased with the increasing incubation time, and tended to a steady value after 40 min (Fig. 4A), which showed the saturated binding of the sandwich immunoreaction. Therefore, 40 min was chosen as the optimal incubation time in the experiment.

The pH of the substrate solution was another important parameter that influenced the enzyme-catalyzed reaction. The pH value was investigated between 6.2 and 8.2. As shown in Fig. 4B, the current change was increased with the increase of pH value from pH 6.2 to 7.4 and then decreased. For lower or higher pH values, a current decrease occurred, probably due to loss or inactivation of the enzyme activity. Therefore, pH 7.4 PBS buffer solution was used as the working buffer solution throughout the experiments.

The concentration of TH and H₂O₂ influenced the performance of the electrochemical enzyme-catalyzed analysis in the measuring system, so that different concentrations of them were analyzed. As shown in Fig. 4C, the peak current of the resulting FCM/AuNPs/HRP-McAb₂/CEA/McAb₁/3D-TG/G-PDDA/GCE increased with the increasing concentrations of TH (curve a) and H₂O₂ (curve b) and tend to stabilization at $50 \mu\text{mol L}^{-1}$ and 3 mmol L^{-1} , respectively. Therefore, $50 \mu\text{mol L}^{-1}$ TH and 3 mmol L^{-1} H₂O₂ were used as the optimal concentrations.

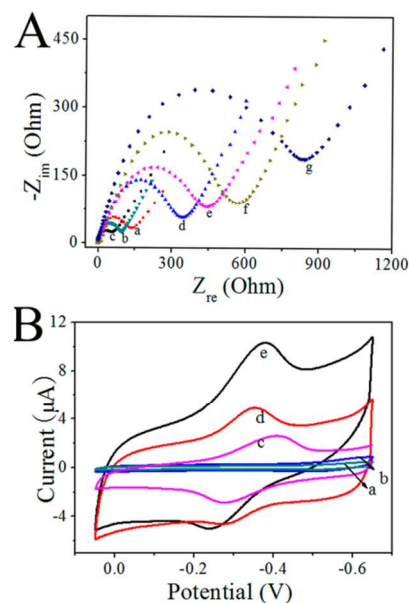


Fig. 3 (A) EIS of (a) bare GCE, (b) G-PDDA/GCE, (c) 3D-TG/G-PDDA/GCE, (d) McAb₁/3D-TG/G-PDDA/GCE, (e) CEA/McAb₁/3D-TG/G-PDDA/GCE, (f) FCM/AuNPs/HRP-McAb₂/CEA/McAb₁/3D-TG/G-PDDA/GCE; (B) CV obtained at (a) 3D-TG/G-PDDA/GCE, (b) McAb₁/3D-TG/G-PDDA/GCE in pH 7.4 PBS, (c) McAb₁/3D-TG/G-PDDA/GCE, (d) HRP/CEA/McAb₁/3D-TG/G-PDDA/GCE, (e) FCM/AuNPs/HRP-McAb₂/CEA/McAb₁/3D-TG/G-PDDA/GCE in pH 7.4 PBS containing $50 \mu\text{mol L}^{-1}$ TH and 3 mmol L^{-1} H₂O₂.

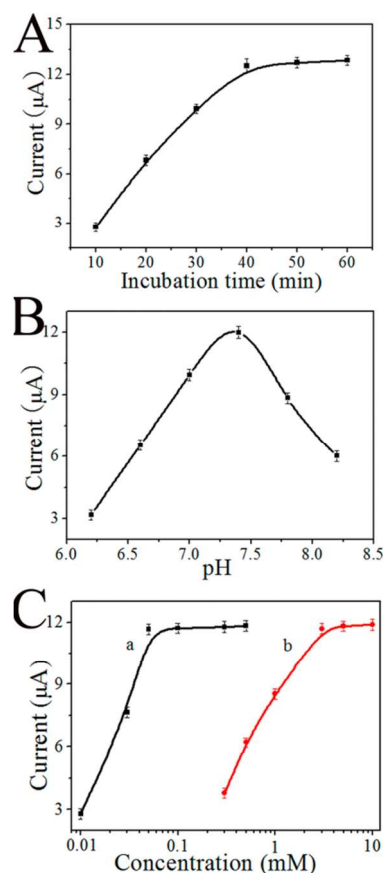


Fig. 4. The effect of (A) incubation time and (B) pH on the DPV responses of the immunosensor toward 5 ng mL^{-1} of CEA; (C) Effect of the concentrations of (a) TH and (b) H₂O₂ on the electrochemical responses.

DPV response

DPV is an electrochemical technique which can show higher sensitivity for determination. Under the optimized experimental conditions, the DPV electro-catalytic current responses were measured by varying the CEA concentration with the HRP-McAb₂/AuNPs/FCM-based sensor as shown in Fig. 5. The peak currents of the immunosensor increased with the increment of CEA concentrations, and exhibited a good linear relationship with logarithm of CEA concentration from 0.0001 to 50 ng mL⁻¹ (Fig. 5A, inset). The linear regression equation (Fig. 5A) was $I = 14.187 + 3.07 \lg [CEA] \text{ (ng} \cdot \text{mL}^{-1}\text{)}$ with a correlation coefficient of 0.9987, and the limit of detection (LOD) at a signal-to-noise of 3σ is 0.026 pg·mL⁻¹ (where σ is the standard deviation of the blank solution, $n=11$). To clearly manifest the reliability of the developed immunoassay, the analytical performance of the proposed electrochemistry immunoassay has been compared with those of other CEA immunoassays, and the results were listed in Table S1 (the detail information on the comparison can be found in the Electronic Supplementary Information). Compared with other methods, the prepared immunoassay had a relatively large linear range and low LOD, which implied the proposed method could be used for the determination of CEA.

To investigate the enhancement effect of immobilizing more HRP on the AuNPs/FCM label, control experiment were carried out under differential pulse voltammetry applying AuNPs/FCM, carbon sphere and graphene sheets as label, respectively. The results displayed that the AuNPs/FCM-labelled electrochemical immunosensor (curve a, Fig. S3) showed higher current and wider linear ranges than carbon sphere and graphene sheets-based electrochemical immunosensors (curve b and c, Fig. S3).

Selectivity, reproducibility and stability of the immunosensor

The selectivity to target analyte is a crucial factor to evaluate the performance of immunosensor. To investigate the selectivity of the immunosensor, the immunosensor was incubated in 0.1 ng·mL⁻¹ of CEA solution containing 10 ng·mL⁻¹ of different interfering agent, such as human chorionic gonadotrophin (HCG), α -fetoprotein (AFP), human immunoglobulin G (IgG) and prostate specific antigen (PSA). As indicated in Fig. 5B, no remarkable change of current was observed in comparison with the result obtained in the presence of CEA only. On the other hand, much weak electrochemistry response was observed by replacing CEA with HCG, AFP, IgG and PSA in the solution, indicating excellent selectivity of the proposed immunosensor.

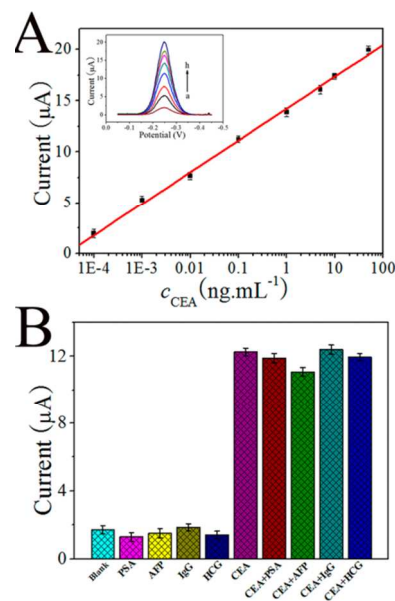


Fig. 5 (A) Calibration curves of the electrochemical immunosensor toward CEA in pH 7.4 PBS containing 50 $\mu\text{mol} \cdot \text{L}^{-1}$ TH and 3 $\text{mmol} \cdot \text{L}^{-1}$ H₂O₂. (inset: peak currents of the immunosensor in the presence of different concentrations of CEA ($\text{ng} \cdot \text{mL}^{-1}$): 0.0001, 0.001, 0.01, 0.1, 1.0, 5.0, 10.0, 50.0, from a to h) (B) Selectivity of the electrochemical immunosensor toward CEA, PSA, AFP, IgG, HCG and their mixture.

Reproducibility was a vital parameter as well. The repeatability and reproducibility of the proposed biosensor were evaluated by intra- and inter-assay coefficients of variation. The intra-assay precision of the analytical method was examined by analyzing three different concentration levels for five replicate determinations. The intra-assay variation coefficients with this method were 4.2%, 3.7% and 5.3% at 5 $\text{ng} \cdot \text{mL}^{-1}$ CEA, respectively. The inter-assay precision was estimated by testing these concentrations with five immunosensors made at the same electrode independently. Similarly, the variation coefficients of the inter-assay precision were 4.6%, 5.1% and 6.0%. The experimental results indicated that the proposed immunosensor was reliable and can be used for CEA detection with acceptable reproducibility.

When the biosensor was not in use, it was stored at 4 °C and the current response was periodically measured. The result showed that no obvious decrease in the response currents to H₂O₂ was observed after two weeks storage, and the current response in the 30th day was more than 90% of the initial current, showing good storage stability. The slow decrease in response seemed to be related to the gradual deactivation of the immobilized antibody incorporated in the composites.

Application in analysis of real serum samples

To evaluate the applicability and reliability of the proposed immunosensor for real serum sample analysis, three clinical serum specimens were tested, which were obtained from the Shandong Tumor Hospital. The results were compared with the reference values obtained by the commercialized available enzyme-linked immunosorbent assay method (ELISA, the detail information on the usage method of the ELISA can be found in the Electronic Supplementary Information). Human serum samples were diluted to different concentrations with a PBS solution of pH 7.0, and each sample was analyzed for five times. As shown in Table 1, the relative error between the two methods ranged from -2.22% to 3.44%. It obviously suggested that there were no significant differences between the results given by the two methods. Meanwhile, the cost of the proposed immunoassay (0.4 dollar for one sample) is close five times lower than the commercialized ELISA (2.2 dollar for one sample). And therefore, the proposed immunoassay could be available for determining CEA in human plasma in the clinical diagnosis.

Table 1 Comparison of serum CEA levels determined using two methods.

| Serum samples | 1 | 2 | 3 |
|---|-------|-------|-------|
| Immunosensor | 10.21 | 27.34 | 42.46 |
| ELISA (ng·mL ⁻¹) ^a | 9.87 | 27.96 | 43.05 |
| Relative error (%) | 3.44 | -2.22 | -1.37 |

^aThe average value of three successive determinations.

Conclusion

In summary, we have successfully designed an ultrasensitive and highly selective immunosensor for the detection of CEA using multi-enzyme labeled nanogold functionalized flower-like hierarchical carbon material as signal amplifying probe. The nanogold functionalized flower-like hierarchical carbon material could be conveniently fabricated through in situ growth of nanogold on carboxylated flower-like hierarchical carbon material and act as desirable carrier with large surface area for efficient immobilization of enzyme and antibodies. In addition, the three-dimensional trepan-like gold/poly (diallyldimethylammonium chloride) functionalized graphene composite modified electrode possessed much larger surface areas and much more active sites to immobilize large amount of capture antibodies in the use of electrochemical signal amplification. Both the signal amplification of HRP/nanogold functionalized flower-like hierarchical carbon material nanoprobe and the electron transfer acceleration of three-dimensional trepan-

like gold/poly (diallyldimethylammonium chloride) functionalized graphene composite greatly improve the sensitivity of the immunoassay method. The proposed immunosensor showed excellent performance for the detection of CEA with a wide linear range, low detection limit and acceptable stability, reproducibility, and accuracy. We anticipate that the fluorescent immunoassay could be extended for determination of other proteins and provide a promising potential in clinical applications.

Acknowledgements

This work was financially supported by the National Natural Science Foundation of China (21475052, 21175058, 21207048), the Natural Science Foundation of Shandong Province, China (ZR2012BZ002), Technology Development Plan of Shandong Province, China (Grant no. 2014GGX103012) and Doctor Foundation of University of Jinan (XBS1428).

Notes and references

^a Key Laboratory of Chemical Sensing & Analysis in Universities of Shandong, School of Chemistry and Chemical Engineering, University of Jinan, Jinan 250022, P. R. China.

^b Shandong Provincial Key Laboratory of Preparation and Measurement of Building Materials, University of Jinan, Jinan 250022, P. R. China.

^c Cancer Research Center, Shandong Tumor Hospital, Jinan 250117, P. R. China.

Electronic Supplementary Information (ESI) available: See DOI: 10.1039/b000000x/

1 H. Kitano, *Science*, 2002, **295**, 1662-1664.

2 V. Kulasingham, E. Diamandis, *Nat. Clin. Pract. Oncol.* 2008, **5**, 588-599.

3 L. Wang, Y. Wang, J.I. Wong, T. Palacios, J. Kong, H.Y. Yang, *Small*, 2014, **10**, 1101-1105.

4 C. Kamrath, H. Böhles, C. Maser-Gluth, *Clini. Chim. Acta*, 2011, **412**, 186-189.

5 Q.L. Lang, F. Wang, L. Yin, M.J. Liu, V. Petrenko, A.H. Liu, *Anal. Chem.*, 2014, **86**, 2767-2774.

6 S. Laing, A. Hernandez-Santana, J. Sassmannshausen, D.L. Asquith, I.B. McInnes, K. Faulds, D. Graham, *Anal. Chem.*, 2011, **83**, 297-302.

7 A.D. Quach, G. Crivat, M.A. Tarr, Z. Rosenzweig, *J. Am. Chem. Soc.*, 2011, **133**, 2028-2030.

8 S. Seo, B. Kim, A. Joe, H. Han, X.Y. Chen, Z. Cheng, E. Jang, *Biomaterials*, 2014, **35**, 3309-3318.

- 9 M.K. Sharma, V.K. Rao, S. Merwyn, G.S. Agarwal, S. Upadhyay, R. Vijayaraghavan, *Talanta*, 2011, **85**, 1812-1817.
- 10 F. Darain, S.U. Park, Y.B. Shim, *Biosens. Bioelectron.*, 2003, **18**, 773-780.
- 11 X.L. Jia, X. Chen, J.M. Han, J. Ma, Z.F. Ma, *Biosens. Bioelectron.*, 2014, **53**, 65-70.
- 12 J.Y. Liu, Y.N. Qin, D. Li, T.S. Wang, Y.Q. Liu, J. Wang, E.K. Wang, *Biosens. Bioelectron.*, 2013, **41**, 436-441.
- 13 G.D. Liu, Y.H. Lin, *Talanta*, 2007, **74**, 308-317.
- 14 X.M. Pei, B. Zhang, J. Tang, B.Q. Liu, D.P. Tang, *Anal. Chin. Acts*, 2013, **758**, 1-18.
- 15 P. Wu, T. Zhao, S.L. Wang, X.D. Hou, *Nanoscale*, 2014, **6**, 43-64.
- 16 C.Y. Chan, Y. Bruemmel, M. Seydack, K.K. Sin, L.W. Wong, E. Merisko-Liversidge, D. Trau, R. Renneberg, *Anal. Chem.*, 2004, **76**, 3638-3645.
- 17 D.P. Tang, J.J. Ren, *Anal. Chem.*, 2008, **80**, 8064-8070.
- 18 Z.Z. Yin, Y. Liu, L.P. Jiang, J.J. Zhu, *Biosens. Bioelectron.*, 2011, **26**, 1890-1894.
- 19 S. Nourani, H. Ghourchian, S.M. Ghourchian, *Anal. Biochem.*, 2013, **441**, 1-7.
- 20 K. Scida, P. Stege, G. Haby, G. Messina, C. García, *Anal. Chin. Acts*, 2011, **691**, 6-17.
- 21 S.S. Cao, L. Fang, Z.Y. Zhao, Y. Ge, S. Piletsky, A. Turner, *Adv. Funct. Mater.*, 2013, **23**, 2162-2167.
- 22 N. Wangoo, C.R. Suri, G. Shekhawat, *Appl. Phys. Lett.*, 2008 **92**, 1331041-1331043.
- 23 Y.Q. Ge, J. Wu, H.X. Ju, S. Wu, *Talanta*, 2014, **120**, 218-223.
- 24 Y.X. Fang, E.K. Wang, *Chem. Comm.*, 2013, **49**, 9526-9539.
- 25 F. Liu, Y. Zhang, S.G. Ge, J.J. Lu, J.H. Yu, X.R. Song, S. Liu, *Talanta*, 2012, **99**, 512-519.
- 26 Y. Zhang, M. Su, L. Ge, S.G. Ge, J.H. Yu, X.R. Song, *Carbon*, 2013, **57**, 22-33.
- 27 Y. Zhang, L. Li, H.M. Yang, Y.N. Ding, M. Su, J.T. Zhu, M. Yan, J.H. Yu, X.R. Song, *RSC Adv.*, 2013, **3**, 14701-14709.
- 28 T.T. Qi, J.F. Liao, Y.S. Li, J.R. Peng, W.T. Li, B.Y. Chu, H. Li, Y.Q. Wei, Z.Y. Qian, *Biosens. Bioelectron.*, 2014, **61**, 245-250.
- 29 S.G. Ge, X.L. Jiao, D.R. Chen, *Analyst*, 2012, **137**, 4440-4447.
- 30 K.P. Liu, J.J. Zhang, G.H. Yang, C.M. Wang, J.J. Zhu, *Electrochem. Commun.*, 2010, **12**, 402-405.
- 31 M. N. Kashid and L. K. Minsker, *Ind. Eng. Chem. Res.*, 2009, **48**, 6465-6469.
- 31 Z.D. Wang, M.S. Bharathi, R. Hariharaputran, H. Xing, L.H. Long, J.H. Li, Y.W. Yang, Y. Lu, *ACS Nano*, 2013, **7**, 2258-2265.
- 32 B.D. Busbee, S.O. Obare, C.J. Murphy, *Adv. Mater.*, 2003, **15**, 414-416.
- 33 Q. Wang, J. Yan, Y.B. Wang, T. Wei, M.L. Zhang, X.Y. Jing, Z.J. Fan, *Carbon*, 2014, **67**, 119-127.
- 34 D.Q. Yang, J.F. Rochette, E. Sacher, *J. Phys. Chem. B*, 2005, **109**, 4481-4484.